Brief Communications

Glutamatergic Transmission Is Sustained at a Later Period of Development of Medial Nucleus of the Trapezoid Body–Lateral Superior Olive Synapses in Circling Mice

Sung Hwa Hong,[1] Myeung Ju Kim,[2] and Seung Cheol Ahn[3]

[1]Department of Otorhinolaryngology–Head and Neck Surgery, Samsung Medical Center, School of Medicine, Sungkyunkwan University, Gangnam-gu, Seoul, Korea 135-710, and Departments of [2]Anatomy and [3]Physiology, College of Medicine, Dankook University, Cheonan, Chungnam, Korea 330-714

Synaptic transmission between the medial nucleus of the trapezoid body (MNTB) and the lateral superior olive (LSO) was investigated in circling mice, an animal model for inherited deafness, using the voltage-clamp technique. In postnatal day 9 (P9)~P11 homozygous (*cir*/*cir*) circling mice, perfusion with 10 μM DL-APV and 10 μM CNQX reduced the 10 min average of postsynaptic currents (PSCs) to 8.8 ± 3.0% compared with controls ($n = 6$). In heterozygous (+/*cir*) mice in the same age range, the 10 min PSCs average was reduced to 87.5 ± 3.7% compared with controls ($n = 7$). In P0~P2 homozygous (*cir*/*cir*) and heterozygous (+/*cir*) mice, the 10 min PSCs averages were 11.0 ± 2.6% ($n = 9$) and 84.1 ± 4.6% ($n = 11$), respectively. The effects of a glutamate antagonist mixture were almost the same in single fiber stimulation of P9~P11 mice, reducing mean PSCs to 5.2 ± 3.1% (homozygous (*cir*/*cir*) mice, $n = 8$) and 78.3 ± 4.3% (heterozygous (+/*cir*) mice, $n = 12$). Immunohistochemical study revealed that glycine receptor (GlyR) immunoreactivity in heterozygous (+/*cir*) mice was more prominent than in homozygous (*cir*/*cir*) mice, while immunoreactivities of NR1 and NR2A-type NMDAR of P16 homozygous (*cir*/*cir*) mice were more prominent than in heterozygous (+/*cir*) mice of the same age. No significant difference was found in the immunoreactivity of NR2B-type NMDAR. These results indicate that glutamatergic transmission is sustained at a later period of developing MNTB–LSO synapses in homozygous (*cir*/*cir*) mice.

Key words: **MNTB; LSO; glutamate; glycine receptor immunoreactivity; NMDA receptor immunoreactivity; circling mice**

Introduction

The LSO, a binaural auditory nucleus in the auditory brainstem, receives GABA/glycinergic inhibitory input from the contralateral ear via the MNTB and excitatory glutamatergic input from the ipsilateral ear through the ventral cochlear nucleus (Boudreau and Tsuchitani, 1968; Moore and Caspary, 1983; Kandler and Friauf, 1995; Kotak et al., 1998). Neurotransmission at immature MNTB–LSO synapses, before hearing onset, differs from mature MNTB–LSO synapses. While MNTB–LSO synapses in mature animals are purely glycinergic (Caspary and Finlayson, 1991; Schwartz, 1992), MNTB–LSO synapses in neonates are both GABAergic and glycinergic (Kotak et al., 1998; Korada and Schwartz, 1999; Nabekura et al., 2004). In addition, immature MNTB–LSO synapses transiently corelease the excitatory neurotransmitter glutamate. Glutamate corelease from MNTB–LSO synapses is most active by P8 in rats (Gillespie et al., 2005).

Abnormalities of the cochlea affect the anatomy and function of the developing and mature auditory system. Cochlear pathology has been associated with a decline in cell number in developing animals (Trune, 1982; Hashisaki and Rubel, 1989), and smaller cell size (Pasic et al., 1994) and reduced protein synthesis (Sie and Rubel, 1992) in mature animals. Neurotransmission is no exception. Cochlear damage and middle ear ossicle removal induce both transient and persistent regulatory changes in transmitter release from glutamatergic, glycinergic, and GABAergic pathways in the mature auditory brainstem (Bledsoe et al., 1995; Potashner et al., 1997, 2000; Suneja et al., 1998).

The circling mouse has recently been identified as an animal model for human deafness (Lee et al., 2001, 2002; Chung et al., 2007). Light microscopic pathology of circling mice shows cochlear degeneration and stereociliary defects of cochlear hair cells observed as early as P10 (Chung et al., 2007). Because spontaneous cochlear degeneration occurs relatively early in circling mice, neurotransmission in the brainstem auditory circuit may differ from that of normal mice. However, neurotransmission in the brainstem auditory circuit, including glutamate corelease previously reported in rats, has not yet been studied in circling mice. The aims of this study were to examine the developmental neurotransmission pattern of MNTB–LSO synapses in circling mice.

Materials and Methods

Animals and slice preparation. Heterozygous females (+/*cir*) were mated with homozygous males (*cir*/*cir*) and their pups were used for this study. The data presented here were obtained from pups between P0~P2 and

Received June 30, 2008; revised Sept. 10, 2008; accepted Oct. 21, 2008.

This work was supported by grants from the Korea Research Foundation (MOEHRD, KRF-2006-E00386) and the Korea Science and Engineering Foundation (KOSEF, R01-2005-000-10739-0), funded by the Korean Government.

Correspondence should be addressed to either of the following: Dr. Seung Cheol Ahn, Department of Physiology, College of Medicine, Dankook University, Room 505, San 29, Anseo-dong, Cheonan, Chungnam, Korea 330-714, E-mail: ansil67@dku.edu; or Dr. Sung Hwa Hong, Department of Otorhinolaryngology–Head and Neck Surgery, Samsung Medical Center, School of Medicine, Sungkyunkwan University, 50 Irwon-dong, Gangnam-gu, Seoul, Korea 135-710, E-mail: shhong@smc.samsung.co.kr.

DOI:10.1523/JNEUROSCI.3002-08.2008

 0270-6474/08/2813003-05$15.00/0

P9~P11. This study was conducted blind, because it was not possible to distinguish between homozygote and heterozygote animals during the period of study. The animals were maintained in the Laboratory Animal Research Center of the Samsung Biomedical Research Institute (SBRI). The Institutional Animal Care and Use Committee (IACUC) of SBRI approved this study. SBRI is a facility accredited by the Association for the Assessment and Accreditation of Laboratory Animal Care International (AAALAC International), which adheres to the guidelines issued by the Institution of Laboratory of Animal Resources (ILAR).

After the mice received deep anesthesia with isoflurane, the brains were removed in ice-cold artificial CSF (aCSF) with 1 mM kynurenic acid, and 300-μm-thick coronal slices were cut with a vibratome (LEICA VT1000s, LEICA Microsystems). The slices were allowed to recover for at least 30 min in an interface chamber before recording. The slices were transferred to a submersion-type chamber mounted on an upright microscope and perfused continuously with Mg^{2+}-free aCSF containing (in mM) NaCl (124), KCl (5), KH_2PO_4 (1.25), glucose (10), $NaHCO_3$ (26), and $CaCl_2$ (2).

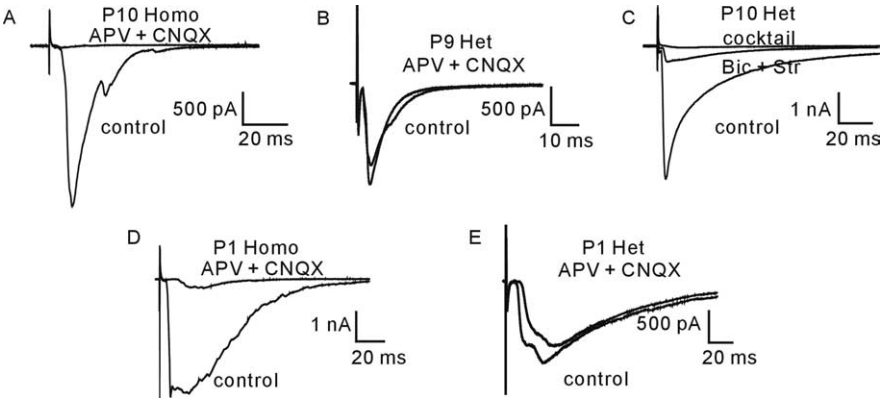

Figure 1. Electrical stimulation of the MNTB elicited glutamatergic PSCs. All of the merged currents presented here are 10 min averages of the PSCs. ***A***, ***D***, In P10 and P1 homozygous (*cir/cir*) mice, MNTB stimulation elicited an inward directed PSC that was almost blocked by the glutamate receptor antagonists DL-APV (10 μM) and CNQX (10 μM). ***B***, ***E***, In P9 and P1 heterozygous (*+/cir*) mice, the PSC elicited by the MNTB stimulation was not sensitive to the same glutamate antagonist mixture. ***C***, In P10 heterozygous (*+/cir*) mice, the PSC elicited by MNTB stimulation was sensitive but not completely blocked by the mixture of a GABA receptor blocker and glycine receptor blocker [10 μM bicuculline (Bic) and 10 μM strychnine (Str)]. The remaining current was blocked by the additional perfusion of a glutamate receptor blocker mixture [cocktail: DL-APV (10 μM) + CNQX (10 μM) + bicuculline (10 μM) + strychnine (10 μM)].

Electrical stimulation and electrophysiology. Low-resistance electrodes (<2 MΩ filled with aCSF), positioned at the lateral end of the MNTB, were used to stimulate LSO inputs (Master 8 and Isoflex, A.M.P.I.). Whole-cell patch-clamp recordings were obtained from the visualized principal type of LSO neurons, as identified by their bipolar morphology. To avoid the remnant effects of previous drug applications, only one cell was tested for every slice. Because we selected the single best slice per mouse, the number of cells presented in the electrophysiological study equaled the number of animals tested. In minimal stimulation experiments, the electrical stimulation intensity was adjusted to ensure a failure rate of >50%. At this intensity, 100~200 responses were evoked at 0.1 Hz. Identification of successful responses and failures was performed off-line by eye. All failures were excluded when calculating average peak amplitudes. The recording electrodes (2–3 MΩ) were filled with solution containing (in mM) K-gluconate (22), EGTA (10), KCl (91), HEPES (20), Na_2GTP (0.3), Na_2ATP (1), KOH (35), and QX-314 (5 mM). The osmolarity was adjusted with sucrose (~285 mOsm) (The Advanced Micro Osmometer Model 3300, Advanced Instruments). All chemicals except QX-314, CNQX, and bicuculline (Tocris) were purchased from Sigma. The data were filtered at 5 kHz (EPC-8, HEKA), digitized at 10 kHz, and stored on a computer using a homemade program (R-clamp 1.23). The analysis of the electrophysiological data and statistical testing were performed with Clampfit 9.2 (Molecular Devices) and Origin 7.0 (OriginLab). Data are expressed as mean ± SEM throughout the text. Comparisons were made using the Student's *t* test, and a *p* value <0.05 was considered statistically significant.

PCR analysis. Tails from the heterozygous or homozygous mice were used for PCR analysis. Genomic DNA was isolated according to the manufacturer's instructions (Bioneer). The absence of the transmembrane inner ear (*tmie*) gene was used to identify the homozygous mice (Mitchem et al., 2002; Naz et al., 2002; Chung et al., 2007). PCR was performed with primers designed to amplify the exon 1 coding region of the *tmie* gene (forward, 5′-AGCTGTAGCTCTGAAATCT-3′; reverse, 5′-TCTGGCAGAATGCATGGAGGCT-3′). Each final reaction volume of 20 μl contained 100 ng of template DNA in 10 mM Tris-HCl (pH 9.0), 40 mM KCl, 1.5 mM $MgCl_2$, 250 mM dNTP, 20 pmol of each primer, and 1 U of *Taq*DNA polymerase (KRP). PCR was performed in an Eppendorf thermocycler (Mastercycler gradient) in two steps. The first step was 4 cycles of denaturation at 96°C for 5 min and annealing at 59°C for 1 min, followed by an extension at 72°C for 1 min. The second step was 30 cycles of denaturation at 96°C for 1 min, annealing at 59°C for 1 min, and extension at 72°C for 1 min, followed by a final extension at 72°C for 10 min at the end of the 30 cycles. Electrophoresis was performed at 93V for 1 h at 25°C. Heterozygous samples were identified by amplification of the *tmie* gene fragment.

Immunohistochemistry. For immunohistochemistry, the animals were perfused transcardially with cold phosphate buffered saline (PBS, 0.02 M, pH 7.4) and ice-cold 4% paraformaldehyde, sequentially. The brains were cryoprotected in a series of cold sucrose solutions and cut into 40 μm sections in the coronal plane. Immunochemistry was performed by the free-floating method, as described previously (Kim et al., 2005). Primary antibodies included rabbit polyclonal anti-NMDAR1 (diluted to 1:500, AB9864, Millipore), rabbit polyclonal anti-NMDAR2A (diluted to 1:1000, 07–632, Millipore), rabbit polyclonal anti-NMDAR2B (diluted to 1:2000, 06–600, Millipore), and rabbit anti-glycine receptor $\alpha_1+\alpha_2$ (diluted to 1:250, ab23809, Abcam) antibodies. Brain sections were incubated overnight at 4°C with diluted primary antibodies in PBS-based blocking buffer containing 1% bovine serum albumin, 0.3% Triton X-100, and 1% normal Horse Serum. After three washes with PBS for 10 min, the sections were incubated with 1:250 diluted secondary antibody (anti-rabbit IgG, Vector laboratory, CA) at room temperature for 1 h. Sections from each group were stained together to eliminate discrepancies caused by different experimental conditions. Sections from the corresponding LSO regions of both homozygous (*cir/cir*) and heterozygous (*+/cir*) mice were selected for analysis. The number of section pairs varied according to the condition of sections. The sections were evaluated using an Olympus BX51 microscope and pictures of the sections were taken with a microscope digital camera system (DP50, Olympus). The NIH image program (Scion Image) was used to determine the staining densities of the receptors. The sum of the gray values of all of the pixels in a selected region was divided by the total number of pixels in the selected region to determine the mean density of receptor immunoreactivity per unit area (mm^{-2}).

Results

Glutamate corelease from MNTB–LSO synapses

P9~P11 mice were evaluated first, because glutamate corelease from MNTB–LSO synapses reportedly decreases after P8 in rats (Gillespie et al., 2005). Postsynaptic currents (PSCs) elicited by the stimulating electrode (located at the MNTB with the frequency of 0.05 Hz) were recorded for 10 min to establish a control, and then 10 μM DL-APV and 10 μM CNQX were perfused into the bath to isolate the glutamate receptor antagonist-sensitive PSCs. We identified two different groups of responses for the PSCs to the mixture of glutamate antagonists (DL-APV +

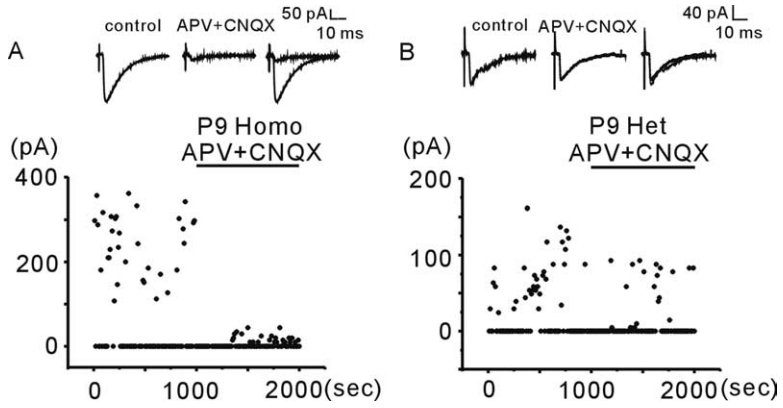

Figure 2. PSCs elicited by minimal stimulation in P9 homozygous (*cir/cir*) (***A***) and heterozygous (+/*cir*) mice (***B***). Successful responses and failures (at 0 current levels) were plotted against time. After 1000 s of control responses elicited at 0.1 Hz, a glutamate antagonist mixture (10 μM DL-APV + 10 μM CNQX) was perfused into the bath, which effectively blocked the PSCs in P9 homozygous (Homo) (*cir/cir*) mice (***A***), but only minimally inhibited the PSCs in P9 heterozygous (Het) (+/*cir*) mice (***B***). The current averages of control responses (left) and post-antagonist application responses (middle) are shown above the plots. The right ones represent merges of the leftmost two current traces.

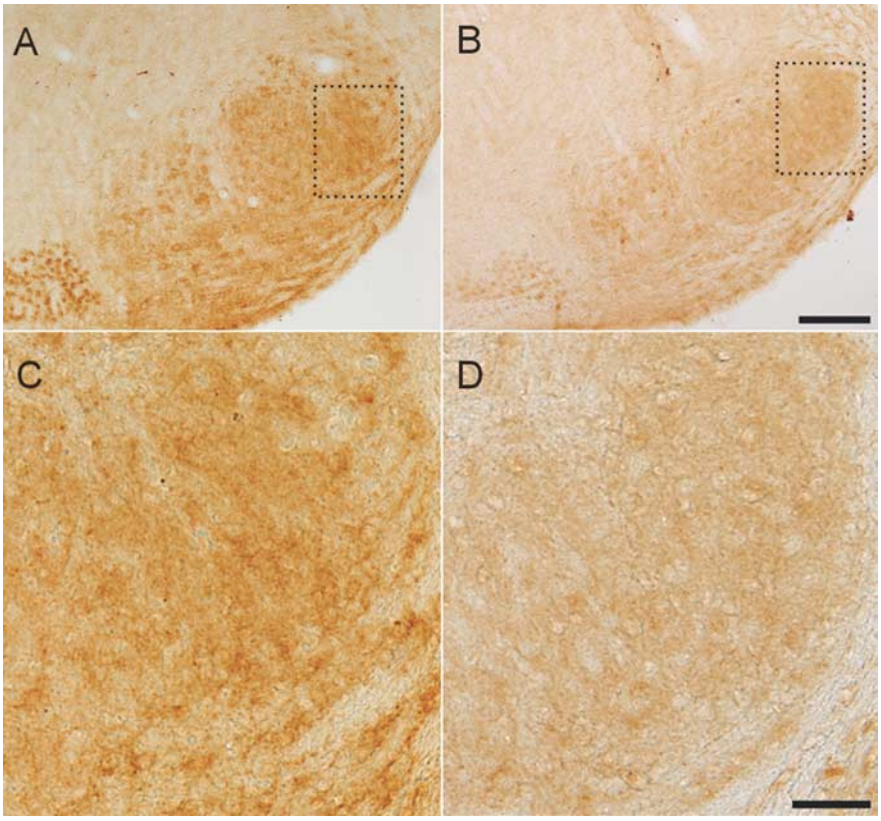

Figure 3. Immunohistochemical localization of GlyR IR (immunoreactivity) in the LSO of P16 heterozygous (+/*cir*) (***A***, ***C***) and homozygous (*cir/cir*) mice (***B***, ***D***). The GlyR IR of the LSO was more prominent in heterozygous (+/*cir*) (***A***, ***C***) than in the homozygous (*cir/cir*) mice (***B***, ***D***). ***C*** and ***D*** are the magnified images of rectangular areas shown in ***A*** and ***B***. Scale bars: ***A***, ***B***, 200 μm, ***C***, ***D***, 50 μm.

CNQX). One was sensitive, but had a partial block of the PSCs (Group 1, 6 of 13 cells), and the other showed a small change in the PSCs (Group 2, 7 of 13 cells). In Group 1, the 10 min average of steady state PSCs after antagonist treatment of the glutamate receptor was 8.8 ± 3.0% of the control ($n = 6$) (Fig. 1*A*), compared with 87.5 ± 3.7% in Group 2 ($n = 7$) (Fig. 1*B*). PCR revealed that Group 1 samples were from homozygous (*cir/cir*) mice, and Group 2 samples were from heterozygous (+/*cir*) mice. The currents remaining after application of bicuculline/strychnine were blocked completely by the application of APV/CNQX (Fig. 1*C*) ($n = 5$) in heterozygous (+/*cir*) mice. A mixture of antagonists (DL-APV + CNQX + bicuculline + strychnine) also blocked the PSCs completely in homozygous (*cir/cir*) mice (data not shown). Bicuculline was not effective in blocking the PSCs of MNTB–LSO synapses in mice older than P9 regardless of genotype (data not shown). In both heterozygous (+/*cir*) and homozygous (*cir/cir*) mice under P8, some portion of the PSCs was inhibited by bicuculline (data not shown), but detailed experiments have not yet been performed. The response latencies after MNTB stimulation in P9~P11 homozygous (*cir/cir*) and heterozygous (+/*cir*) mice were 2.8 ± 0.2 ms ($n = 6$) and 2.5 ± 0.2 ms ($n = 7$), respectively, ruling out the activation of a disynaptic pathway between the MNTB and LSO.

Because glutamate corelease from MNTB–LSO synapses is a developmental process in rats, we repeated the same experiments in P0~P2 mice. Contrary to our expectations, the results are almost identical with those obtained from P9~P11 mice. The mixture of glutamate antagonists (10 μM DL-APV + 10 μM CNQX) reduced the 10 min average of steady state PSCs to 11.0 ± 2.6% of the control ($n = 9$) (Fig. 1*D*) in homozygous (*cir/cir*) mice, and 84.1 ± 4.6% in heterozygous (+/*cir*) mice ($n = 11$) (Fig. 1*E*). There was no significant difference between the results obtained from either heterozygous (+/*cir*) or homozygous (*cir/cir*) P9~P11 and P0~P2 mice, indicating that the pattern of neurotransmission at MNTB–LSO synapses changes very little by P11.

For the next step, we investigated whether glutamate and GABA/glycine are released from the same populations of MNTB neurons using minimal stimulation techniques (Kim and Kandler, 2003; Gillespie et al., 2005). In slices obtained from P9~P11 mice, minimal stimulation elicited PSCs of variable amplitudes (homozygous (*cir/cir*): 54~322 pA, $n = 8$, heterozygous (+/*cir*): 28~663 pA, $n = 12$). Although the PSCs of homozygous (*cir/cir*) mice (Fig. 2*A*) were larger than those of heterozygous (+/*cir*) mice (Fig. 2*B*), the average PSCs of both groups were not significantly different (independent *t* test, 159.7 ± 31.8 pA [$n = 8$, homozygous (*cir/cir*)], 195.8 ± 62.2 pA [$n = 12$, heterozygous (+/*cir*)]). As with multifiber stimulation, the effects of glutamate antagonists were almost identical in single fiber stimulation. In homozygous (*cir/cir*) mice, the average PSC (159.7 ± 31.8 pA) was reduced to 7.6 ± 4.3 pA ($n = 8$, 5.2 ± 3.1% compared with the control) (Fig. 2*A*) by the glutamate

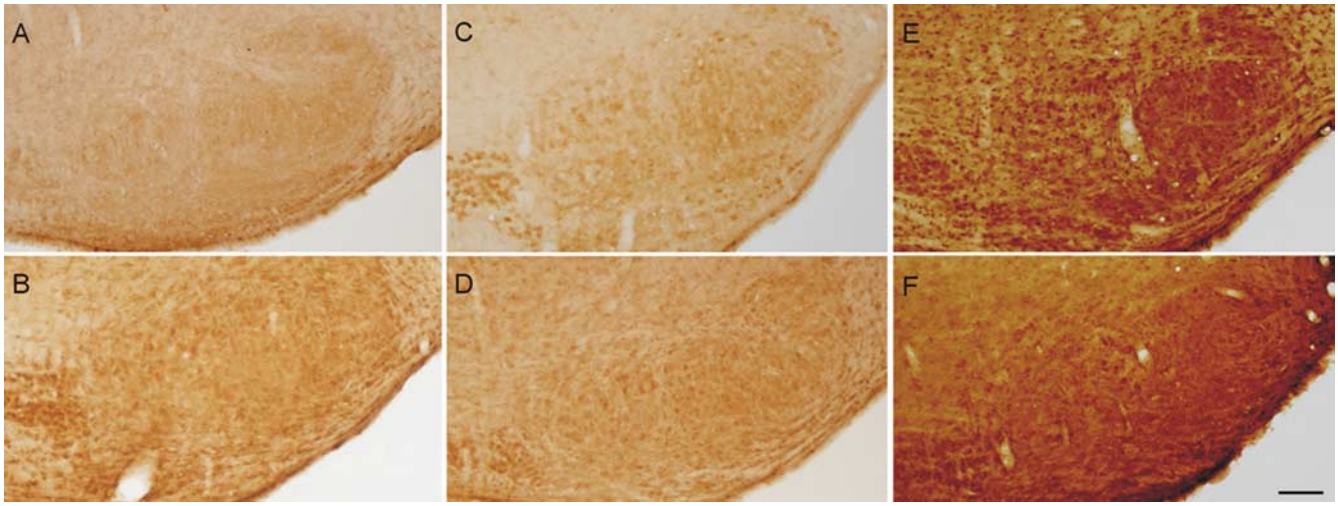

Figure 4. Immunohistochemical localization of NR1 (***A***, ***B***), NR2A (***C***, ***D***), and NR2B (***E***, ***F***) in the LSO of P16 heterozygous (+/*cir*) (***A***, ***C***, ***E***) and homozygous (*cir/cir*) mice (***B***, ***D***, ***F***). Both NR1 and NR2A IR were more prominent in homozygous (*cir/cir*) (***B***, ***D***) than in heterozygous (+/*cir*) mice (***A***, ***C***). No significant difference was found in NR2B IR between heterozygous (+/*cir*) (***E***) and homozygous (*cir/cir*) (***F***) mice. Scale bars: ***A–F***, 100 μm.

antagonist mixture (10 μM DL-APV + 10 μM CNQX). In five of eight cells from homozygous (*cir/cir*) mice, the glutamate antagonist mixture blocked PSCs completely (data not shown). In the remaining 3 cells, the average PSC was reduced to 13.6 ± 5.7%. This finding indicates that some MNTB fibers are purely glutamatergic and others are not. In heterozygous (+/*cir*) mice, the glutamate antagonist mixture significantly reduced the average PSC (195.8 ± 62.2 pA) to 143.4 ± 41.6 pA (paired *t* test, $p < 0.05$, $n = 12$, 78.3 ± 4.3% compared with control), but there was no fiber showing a complete block of PSCs by the glutamate antagonist mixture. These data suggests that glutamate can be released from GABA/glycinergic MNTB–LSO synapses in heterozygous (+/*cir*) mice, although not as much as in homozygous (*cir/cir*) mice.

Comparison of glycine receptor and NMDA receptor immunoreactivities

The glycinergic portion of the PSCs was only 8.8 ± 3.0% in P9~P11 homozygous (*cir/cir*) mice, suggesting the possibility of underdevelopment of GlyR in the LSO of the homozygous (*cir/cir*) mice. Accordingly, we investigated the density of the GlyR α subunit in the LSO of both homozygous (*cir/cir*) and heterozygous (+/*cir*) mice by immunohistochemistry at age P16. GlyR immunoreactivity in the LSO was more prominent in heterozygous (+/*cir*) mice than in homozygous (*cir/cir*) mice (Fig. 3). The mean densities of LSO GlyR immunoreactivity in 10 paired slices (total 20 slices) from 6 mice (3 heterozygous (+/*cir*) and 3 homozygous (*cir/cir*) mice) were 48.3 ± 4.6 and 23.2 ± 3.9 (mm^{-2}), respectively (independent *t* test, $p < 0.05$). We next investigated whether there were differences in glutamate receptor immunoreactivities between homozygous (*cir/cir*) and heterozygous (+/*cir*) mice. The NMDAR antagonist DL-APV abolished a large portion of the glutamatergic PSCs in P9~P11 mice regardless of genotype (data not shown), and so we focused on the immunoreactivities of NR1, NR2A, and NR2B, which are the subunits of NMDAR. In stark contrast to GlyR, LSO NR immunoreactivities of homozygous (*cir/cir*) mice were not weaker than those of heterozygous (+/*cir*) mice at P16 (Fig. 4). The mean densities of the heterozygous and homozygous LSO immunoreactivity of 14 paired slices (28 slices total) from 10 mice [5 heterozygous (+/*cir*) and 5 homozygous (*cir/cir*) mice] were 32.6 ± 2.8 and 49.6 ± 4.5 (mm^{-2}), respectively, for NR1, 28.4 ± 2.4 and 55.4 ± 7.8 (mm^{-2}), respectively (16 paired slices for a total of 32 slices), from 10 mice (5 homo + 5 hetero) for NR2A, and 94.5 ± 5.8 and 94.6 ± 8.2 (mm^{-2}), respectively (10 paired slices for a total of 20 slices), from 10 mice (5 homo + 5 hetero) for NR2B. The mean densities of NR1 and NR2A immunoreactivities of homozygous (*cir/cir*) mice were significantly greater than those of heterozygous (+/*cir*) mice (independent *t* test, $p < 0.05$). Both the immunohistochemical data and electrophysiological data indicate that glutamate is a major neurotransmitter in MNTB–LSO synapses of homozygous (*cir/cir*) mice.

Discussion

In rats, glutamate corelease gradually declines after P8 (Gillespie et al., 2005). The situation is quite different in circling mice (homozygous (*cir/cir*) mice), where the major neurotransmitter at MNTB–LSO synapses is glutamate, not glycine, at least by P11. The difference between rats and circling mice was clearly seen in our minimal stimulation experiment, in which we observed purely glutamatergic responses. We saw two different PSC responses in homozygous (*cir/cir*) mice: a large but partial inhibition and complete inhibition by a glutamate antagonist mixture. These two responses indicate that there might be at least two types of MNTB fibers, such as purely glutamatergic and glutamate/GABA/glycinergic. It remains unclear whether these two types of fibers belong to different populations of MNTB fibers, because the purely glutamatergic MNTB fibers could be the final state of the glutamate/GABA/glycinergic MNTB fibers.

Some mouse strains with genetic neonatal hypothyroidism display retarded maturation of the cochlear structures, leading to morphologic and electrophysiologic cochlear abnormalities and hearing deficits (Rusch et al., 2001; Karolyi et al., 2007). These findings support the possibility that the sustained glutamatergic transmission in homozygous (*cir/cir*) mice merely reflects the temporary, immature state of MNTB–LSO synapses. We do not know whether the maturation of MNTB–LSO synapses takes place normally in homozygous (*cir/cir*) mice compared with heterozygous (+/*cir*) littermates. However, studies reporting normal projections between auditory nuclei (Youssoufian et al., 2008) and auditory nerve-independent development of synaptic strength at the calyx of Held in congenitally deaf (dn/dn) mice

(Youssoufian et al., 2005) suggest the possibility of normal maturation of MNTB–LSO synapses in homozygous (*cir/cir*) mice. The neurotransmitter shift from glutamate to glycine in adult homozygous (*cir/cir*) mice still needs further investigation.

The signals and mechanisms that initiate and mediate the cessation of glutamatergic corelease in rats are not known well. At the beginning of the experiment, since organs of Corti completely disappear along most of the length of the cochlea as early as P21 in homozygous (*cir/cir*) mice (Chung et al., 2007), we hypothesized that the gradual weakening of the spontaneous synaptic activity from the cochlea would hinder the neurotransmitter switch from glutamate to glycine. Although it is generally accepted that synaptic activity affects synaptic development (Katz and Shatz, 1996; Friauf and Lohmann, 1999), the similar glycinergic portions of PSCs we observed between P0∼P2 and P9∼P11 do not support our hypothesis. Because the observation period was too short and the cochlea deteriorated gradually, additional studies of early complete deafferentation of normal rats or mice are needed to determine the effect of spontaneous synaptic activity on sustained glutamatergic transmission.

The similarities between the mouse and human genomes, and between the physiology and morphology of their auditory systems, have made mouse models a major tool for the investigation of human congenital deafness (Ahituv and Avraham 2002). In this study, we found sustained glutamatergic transmission between MNTB–LSO synapses at a later period of development. These results might help elucidate the central changes underlying human hereditary deafness.

References

Ahituv N, Avraham KB (2002) Mouse models for human deafness: current tools for new fashions. Trends Mol Med 8:447–451.

Bledsoe SC Jr, Nagase S, Miller JM, Altschuler RA (1995) Deafness-induced plasticity in the mature central auditory system. Neuroreport 7:225–229.

Boudreau JC, Tsuchitani C (1968) Binaural interaction in the cat superior olive S segment. J Neurophysiol 31:442–454.

Caspary DM, Finlayson PG (1991) Superior olivary complex: functional neuropharmacology of the principal cell types. In: Neurobiology of hearing: the central auditory system (Altschuler RA, Bobbin RP, Clopton BM, Hoffman DW, eds), pp 141–161. New York: Raven.

Chung WH, Kim KR, Cho YS, Cho DY, Woo JH, Ryoo ZY, Cho KI, Hong SH (2007) Cochlear pathology of the circling mouse: a new mouse model of DFNB6. Acta Otolaryngol 127:244–251.

Friauf E, Lohmann C (1999) Development of auditory brainstem circuitry. Activity-dependent and activity-independent processes. Cell Tissue Res 297:187–195.

Gillespie DC, Kim G, Kandler K (2005) Inhibitory synapses in the developing auditory system are glutamatergic. Nat Neurosci 8:332–338.

Hashisaki GT, Rubel EW (1989) Effects of unilateral cochlea removal on anteroventral cochlear nucleus neurons in developing gerbils. J Comp Neurol 283:5–73.

Kandler K, Friauf E (1995) Development of glycinergic and glutamatergic synaptic transmission in the auditory brainstem of perinatal rats. J Neurosci 15:6890–6904.

Karolyi IJ, Dootz GA, Halsey K, Beyer L, Probst FJ, Johnson KR, Parlow AF, Raphael Y, Dolan DF, Camper SA (2007) Dietary thyroid hormone replacement ameliorates hearing deficits in hypothyroid mice. Mamm Genome 18:596–608.

Katz LC, Shatz CJ (1996) Synaptic activity and the construction of cortical circuits. Science 274:1133–1138.

Kim G, Kandler K (2003) Elimination and strengthening of glycinergic/GABAergic connections during tonotopic map formation. Nat Neurosci 6:282–290.

Kim MJ, Shin KS, Chung YB, Jung KW, Cha CI, Shin DH (2005) Immunohistochemical study of p47Phox and gp91Phox distribution in rat brain. Brain Res 1040:178–186.

Korada S, Schwartz IR (1999) Development of GABA, glycine, and their receptors in the auditory brainstem of gerbil: a light and electron microscopic study. J Comp Neurol 409:664–681.

Kotak VC, Korada S, Schwartz IR, Sanes DH (1998) A developmental shift from GABAergic to glycinergic transmission in the central auditory system. J Neurosci 18:4646–4655.

Lee JW, Lee EJ, Hong SH, Chung WH, Lee HT, Lee TW, Lee JR, Kim HT, Suh JG, Kim TY, Ryoo ZY (2001) Circling mouse: possible animal model for deafness. Comp Med 51:550–554.

Lee JW, Ryoo ZY, Lee EJ, Hong SH, Chung WH, Lee HT, Chung KS, Kim TY, Oh YS, Suh JG (2002) Circling mouse, a spontaneous mutant in the inner ear. Exp Anim 51:167–171.

Mitchem KL, Hibbard E, Beyer LA, Bosom K, Dootz GA, Dolan DF, Johnson KR, Raphael Y, Kohrman DC (2002) Mutation of the novel gene Tmie results in sensory cell defects in the inner ear of spinner, a mouse model of human hearing loss DFNB6. Hum Mol Genet 11:1887–1898.

Moore MJ, Caspary DM (1983) Strychnine blocks binaural inhibition in lateral superior olivary neurons. J Neurosci 3:237–242.

Nabekura J, Katsurabayashi S, Kakazu Y, Shibata S, Matsubara A, Jinno S, Mizoguchi Y, Sasaki A, Ishibashi H (2004) Developmental switch from GABA to glycine release in single central synaptic terminals. Nat Neurosci 7:17–23.

Naz S, Giguere CM, Kohrman DC, Mitchem KL, Riazuddin S, Morell RJ, Ramesh A, Srisailpathy S, Deshmukh D, Riazuddin S, Griffith AJ, Friedman TB, Smith RJ, Wilcox ER (2002) Mutations in a novel gene, TMIE, are associated with hearing loss linked to the DFNB6 locus. Am J Hum Genet 71:632–636.

Pasic TR, Moore DR, Rubel EW (1994) Effect of altered neuronal activity on cell size in the medial nucleus of the trapezoid body and ventral cochlear nucleus of the gerbil. J Comp Neurol 348:111–120.

Potashner SJ, Suneja SK, Benson CG (1997) Regulation of D-aspartate release and uptake in adult brain stem auditory nuclei after unilateral middle ear ossicle removal and cochlear ablation. Exp Neurol 148:222–235.

Potashner SJ, Suneja SK, Benson CG (2000) Altered glycinergic synaptic activities in guinea pig brain stem auditory nuclei after unilateral cochlear ablation. Hear Res 147:125–136.

Rusch A, Ng L, Goodyear R, Oliver D, Lisoukov I, Vennstrom B, Richardson G, Kelley MW, Forrest D (2001) Retardation of cochlear maturation and impaired hair cell function caused by deletion of all known thyroid hormone receptors. J Neurosci 21:9792–9800.

Schwartz IR (1992) The superior olivary complex and lateral lemniscal nuclei. In: The mammalian auditory pathways: neuroanatomy (Webster B, Popper AN, Fay RR, eds), pp 117–167. New York: Springer.

Sie KC, Rubel EW (1992) Rapid changes in protein synthesis and cell size in the cochlear nucleus following eighth nerve activity blockade or cochlear ablation. J Comp Neurol 320:501–508.

Suneja SK, Potashner SJ, Benson CG (1998) Plastic changes in glycine and GABA release and uptake in adult brain stem auditory nuclei after unilateral middle ear ossicle removal and cochlear ablation. Exp Neurol 151:273–288.

Trune DR (1982) Influence of neonatal cochlear removal on the development of mouse cochlear nucleus: I. Number, size, and density of its neuron. J Comp Neurol 209:409–424.

Youssoufian M, Oleskevich S, Walmsley B (2005) Development of a robust central auditory synapse in congenital deafness. J Neurophysiol 94:3168–3180.

Youssoufian M, Couchman K, Shivdasani MN, Paolini AG, Walmsley B (2008) Maturation of auditory brainstem projections and calyces in the congenitally deaf (dn/dn) mouse. J Comp Neurol 506:442–451.